Applied Physics Letters

Defect accommodation in off-stoichiometric $(SrTiO_3)_nSrO$ Ruddlesden–Popper superlattices studied with positron annihilation spectroscopy

Cite as: Appl. Phys. Lett. **117**, 062901 (2020); https://doi.org/10.1063/5.0011136
Submitted: 17 April 2020 • Accepted: 25 June 2020 • Published Online: 12 August 2020

Natalie M. Dawley, Berit H. Goodge, Werner Egger, et al.

Applied Physics Letters ARTICLE scitation.org/journal/apl

Defect accommodation in off-stoichiometric $(SrTiO_3)_nSrO$ Ruddlesden–Popper superlattices studied with positron annihilation spectroscopy

Cite as: Appl. Phys. Lett. **117**, 062901 (2020); doi: 10.1063/5.0011136
Submitted: 17 April 2020 · Accepted: 25 June 2020 ·
Published Online: 12 August 2020

View Online Export Citation CrossMark

Natalie M. Dawley,[1] Berit H. Goodge,[2,3] Werner Egger,[4] Matthew R. Barone,[1] Lena F. Kourkoutis,[2,3] David J. Keeble,[5] and Darrell G. Schlom[1,3,6,a)]

AFFILIATIONS

[1]Department of Materials Science and Engineering, Cornell University, Ithaca, New York 14853, USA
[2]School of Applied and Engineering Physics, Cornell University, Ithaca, New York 14853, USA
[3]Kavli Institute at Cornell for Nanoscale Science, Ithaca, New York 14853, USA
[4]Universität Bundeswehr München, D-85577 Neubiberg, Germany
[5]Carnegie Laboratory of Physics, SUPA, School of Science and Engineering, University of Dundee, Dundee DD1 4HN, United Kingdom
[6]Leibniz-Institut für Kristallzüchtung, 12489 Berlin, Germany

[a)]**Author to whom correspondence should be addressed:** schlom@cornell.edu

ABSTRACT

The low dielectric loss underlying the record performance of strained $(SrTiO_3)_nSrO$ Ruddlesden–Popper films as tunable microwave dielectrics was postulated to arise from $(SrO)_2$ faults accommodating local non-stoichiometric defects. Here, we explore the effect of non-stoichiometry on $(SrTiO_3)_nSrO$ using positron annihilation lifetime spectroscopy on a composition series of 300 nm thick $n = 6$ $(Sr_{1+\delta}TiO_3)_nSrO$ thin films. These films show titanium-site vacancies across the stoichiometry series, with evidence that TiO_x vacancy complexes dominate. Little change in defect populations is observed across the series, indicating the ability of Ruddlesden–Popper phases to accommodate ± 5% off-stoichiometry. This ability for defect accommodation is corroborated by scanning transmission electron microscopy with electron energy loss spectroscopy.

Defects play a key role in understanding and engineering materials. In the $n = \infty$ parent phase of Ruddlesden–Popper $(SrTiO_3)_nSrO$, pure $SrTiO_3$, intrinsic point defects can dramatically affect properties: oxygen-reduced samples induce *n*-type conduction,[1] off-stoichiometric point defects decrease thermal conductivity,[2–4] and ferroelectricity can emerge for ultrathin films due to nanopolarized intrinsic point defects.[5] The quantitative prediction,[6,7] identification, and measurement of these defects in $SrTiO_3$ thin films are challenging. For titanium-rich films, it is known that there is a corresponding increase in strontium vacancies, titanium antisite defects, and amorphous TiO_2-rich regions.[8–11] For strontium-rich $SrTiO_3$, it is well known that $(SrO)_2$ faults accommodate the strontium-excess forming disordered $(SrTiO_3)_nSrO$ Ruddlesden–Popper phases.[12–14] This has been observed in thin films of off-stoichiometric $SrTiO_3$[15–18] and in bulk $SrTiO_3$, where $(SrO)_2$ faults are observed with strontium excess of >0.01 at. %.[19,20] It is yet to be explored how the $(SrO)_2$ faults affect the vacancy populations in $(SrTiO_3)_nSrO$ or strontium-rich $SrTiO_3$. Ruddlesden–Popper superlattices have gained interest in recent years for their superconducting,[21–24] colossal magnetoresistive,[25] ferroelectric,[26–30] and tunable dielectric[31,32] properties and use as cathodes in solid fuel cells,[33] without full elucidation of the defect mechanisms in these materials. When epitaxially strained, these superlattice structures have the highest reported figure of merit for high-frequency tunable dielectrics,[31,32] at variance to the high loss seen in their titanate counterparts, $SrTiO_3$, $BaTiO_3$, and $(Ba,Sr)TiO_3$.[34–36] Because loss at these gigahertz frequencies is caused by extrinsic defects, notably charged point defects, high figures of merit indicate their absence in these superlattices.

In $SrTiO_3$, Ruddlesden–Popper non-stoichiometric defects are hypothesized[31] to be accommodated by growth (strontium excess) or reduction (titanium excess) of $(SrO)_2$ planar faults, which have a lower formation energy than that of a point defect.[37] Here, using positron

annihilation lifetime spectroscopy (PALS), we examine how Ruddlesden–Popper structures accommodate off-stoichiometry when $Sr_{1+\delta}TiO_3$ is inserted into an $n = 6$ $(SrTiO_3)_nSrO$ structure grown by oxide molecular-beam epitaxy (MBE). We have used PALS previously to examine pulsed-laser deposited (PLD) 200 nm thick titanium-rich $SrTiO_3$ films and found a clear trend in the presence of both strontium and titanium vacancies.[9,10] In titanium-rich $SrTiO_3$ thin films grown homoepitaxially by PLD on (001) $SrTiO_3$ substrates, strontium vacancies were found to dominate, crossing over to a higher proportion of titanium vacancies as the films became more stoichiometric. All films had vacancy concentrations >50 ppm.

300 nm thick $n = 6$ $(Sr_{1+\delta}TiO_3)_nSrO$ films with a range of compositions ($\delta = \pm$ 5%) were grown on (001) $SrTiO_3$ single crystal substrates. Films were deposited using a Veeco GEN10 MBE chamber at 900 °C (as measured by the substrate thermocouple, which is not in direct contact with the substrate; the true substrate temperature is around 800 °C) at an oxidant background pressure of 1×10^{-6} Torr O_2 + ~10% O_3. Atomic layering was achieved by elemental source shuttering and calibration of individual SrO and TiO_2 monolayer shutter times using reflection high-energy electron diffraction (RHEED) intensity oscillations.[38–40] The strontium shutter time was then increased or decreased by the desired off-stoichiometry percentage for the strontium layers within the $SrTiO_3$ portion of $(Sr_{1+\delta}TiO_3)_nSrO$ to achieve the $\delta \pm$ 5% Sr/Ti ratio.

Samples were characterized by x-ray diffraction as seen in Fig. 1(a). As the films become further off-stoichiometric, the diffraction peaks begin to split, indicating a loss in superlattice periodicity. This occurs more rapidly for titanium-rich films than strontium-rich

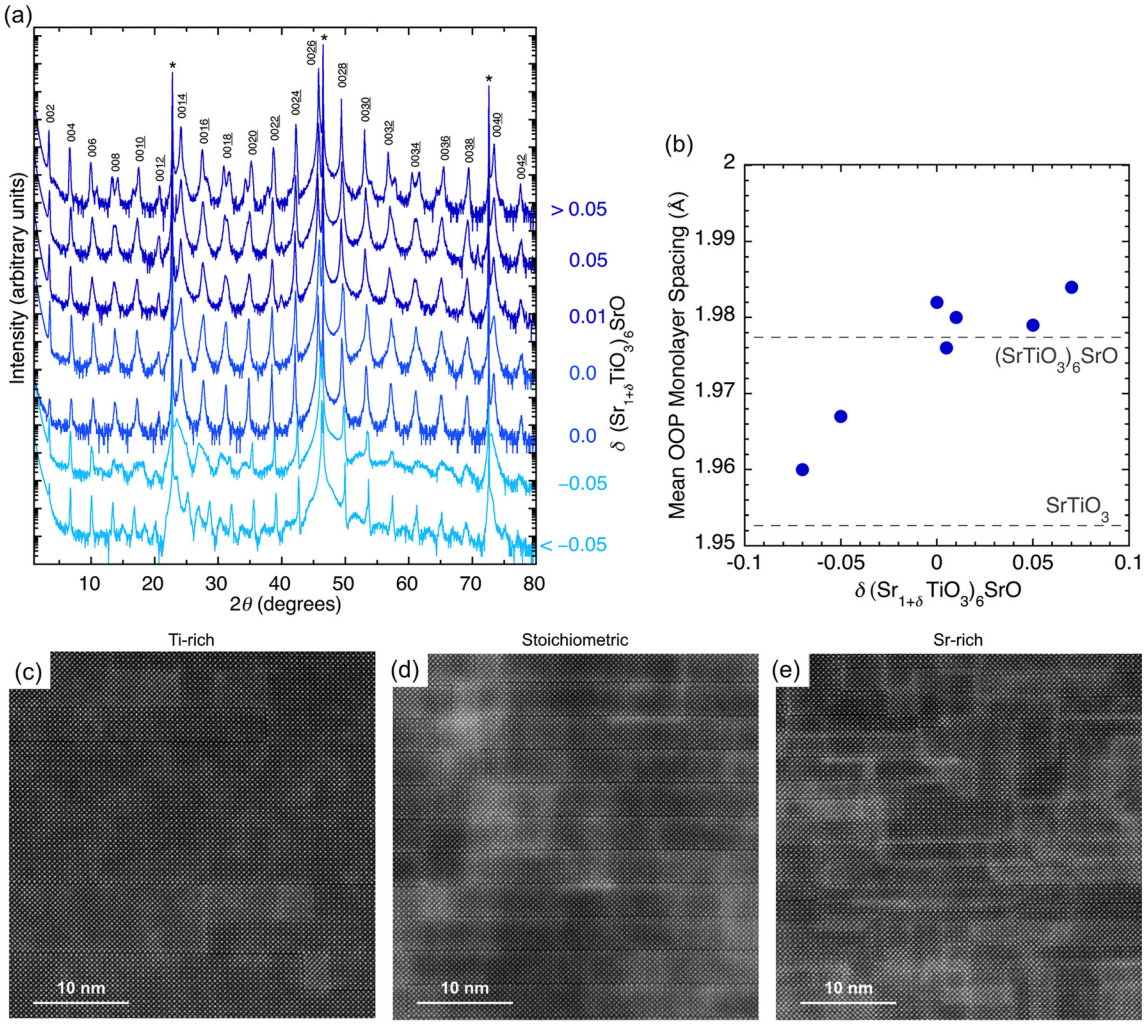

FIG. 1. (a) X-ray diffraction of $\delta = \pm$ 5% of 300 nm thick $n = 6$ $(Sr_{1+\delta}TiO_3)_nSrO$ films grown on (001) $SrTiO_3$. The diffraction-peak periodicity degrades with the increasing off-composition. The (001) $SrTiO_3$ substrate peaks are labeled with an asterisk (∗). (b) The mean out-of-plane (OOP) monolayer spacing of $n = 6$ $(Sr_{1+\delta}TiO_3)_nSrO$ films calculated from the 0026 peak. The *y*-axis error is the size of the plot markers. (c)–(e) Representative atomic-resolution MAADF-STEM images of three $(Sr_{1+\delta}TiO_3)_nSrO$ films show how off-stoichiometry is accommodated structurally through the (c) removal (titanium-rich with $\delta \sim -0.05$) or (e) addition (strontium-rich with $\delta \sim +0.05$) of SrO planes as compared to (d) a stoichiometric sample.

films. All films have narrow ω rocking curves with a full-width-at-half-maximum (FWHM) comparable to the underlying substrate < 34 arc sec (0.009°) (not shown). The low FWHM of these films attests to the defect accommodating nature of $(SrTiO_3)_nSrO$ despite portions of the samples being off-stoichiometric by > 5%. The main superlattice peak, 0026, is a good measure of the average out-of-plane (OOP) spacing, i.e., the average spacing between SrO and TiO_2 cation layers along the [001] direction, and is plotted in Fig. 1(b).[36] The spacing between two SrO layers is larger than that of TiO_2 and SrO layers, and so higher average monolayer spacing indicates more horizontal SrO layers in the film. The average spacing between monolayers decreases sharply in strontium-deficient (titanium-rich) films due to fewer in-plane $(SrO)_2$ faults. In the strontium-rich regime, we do not see the same average monolayer spacing increase, likely because the additional $(SrO)_2$ faults that form are primarily oriented vertically (parallel to the direction of film growth).

Detailed investigation into the structure of these films was conducted using atomic-resolution scanning transmission electron microscopy (STEM). Cross-sectional samples of the titanium-rich ($\delta \sim -0.05$), stoichiometric, and strontium-rich ($\delta \sim +0.05$) films seen in Figs. 1(c)–1(e) were prepared to thicknesses of ~20 nm using the standard focused ion beam (FIB) lift-out method on a Thermo Scientific Helios G4 UX FIB. The samples were imaged on an aberration-corrected FEI Titan Themis at 120 kV with a probe convergence semi-angle of 21.4 mrad. Inner and outer collection angles of 36 and 107 mrad were used to collect medium-angle annular dark field (MAADF)-STEM images, respectively, revealing the atomic structure of the films, shown in Figs. 1(c)–1(e). In addition to the high-angle *Z*-contrast that distinguishes between heavy and light nuclei, the lower collection angles included in MAADF-STEM also contribute some diffraction contrast in the resulting images. Signatures of local crystallographic strain fields can be observed where brightening of the background highlights planar defects in the lattice.

Electron energy loss spectroscopy (EELS) mapping was also performed using the same Titan system equipped with a 965 GIF Quantum ER and Gatan K2 Summit detector operated in electron counting mode, with a beam current of ~30 pA and scan times of 2.5–5 ms per 0.4 Å pixel.

To identify vacancies in the $n = 6$ $(Sr_{1+\delta}TiO_3)_nSrO$ thin-film stoichiometry series, we measured vacancy populations using variable-energy positron annihilation lifetime spectroscopy (VE-PALS). Positrons implanted in the films rapidly thermalize and then annihilate with a bulk lattice or defect state, with a characteristic lifetime τ_i and probability I_i. The positron annihilation event emits two simultaneous γ-rays, one of which is detected. The time intervals with respect to the arrival of the positrons form the lifetime spectrum. By analyzing the lifetime spectrum, the positron lifetime components, characteristic of the bulk (perfect lattice) or defect states, are extracted. The positron trapping probability of a defect depends on its charge and open volume size; more negatively charged vacancy defects, such as strontium and titanium vacancies, trap more strongly. VE-PALS measurements were performed on the $n = 6$ $(Sr_{1+\delta}TiO_3)_nSrO$ films using the neutron induced positron beamline (NEPOMUC) operated by FRM II at Heinz Maier-Leibnitz Zentrum (MLZ), Garching.[41,42] The positron lifetime spectra were measured using position implantation energies of 5 or 6 keV, giving a calculated mean implantation depth of 100–140 nm in $SrTiO_3$.[9,10] The spectrometer was set to have a 40 ns time window, and each spectrum contained 4×10^6 counts. From a four-term free fit of the resulting spectra, the dominant state is shown for each film in Fig. 2 compared to the characteristic lifetime of possible $SrTiO_3$ vacancy states. Characteristic lifetime calculations have not been performed for the $n = 6$ $(SrTiO_3)_nSrO$ system, and so the values for vacancies in $SrTiO_3$ are used from Refs. 9 and 43 or calculated from defect structures in $SrTiO_3$ reported in Ref. 6 (also see the supplementary material) using the MIKA/DOPPLER package for density functional theory.[44] For this work, the positron lifetime in bulk $n = 6$ $(SrTiO_3)_nSrO$ was calculated for a geometrically relaxed structure. The strontium, titanium, and titanium-oxygen vacancies are geometrically symmetric in the $SrTiO_3$ unit cell. For the titanium-dioxygen vacancy, only a linear O–Ti–O vacancy defect was considered.

If $(SrO)_2$ Ruddlesden–Popper faults do not accommodate off-stoichiometry, we would expect the titanium rich-films, $\delta < 0$, to have higher strontium vacancy concentrations, which would produce a high dominant positron lifetime in the range of 280–290 ps as shown in Refs. 9 and 10. In contrast, dominant lifetimes for the $n = 6$ $(Sr_{1+\delta}TiO_3)_nSrO$ films show little variance and are clustered between 218 and 230 ps (Fig. 2), around the TiO_x vacancy lifetimes, contributing > 70% of the total spectra intensity (see supplementary material Table I). While it is non-trivial to distinguish the contribution of each $(V_{Ti}''''2V_O^{\bullet\bullet})^x$, $(V_{Ti}''''V_O^{\bullet\bullet})''$, and τ_{RP6}, the bulk state of pure $(SrTiO_3)_6SrO$, it is clear that TiO_x vacancies are the dominant vacancies found in $n = 6$ $(Sr_{1+\delta}TiO_3)_nSrO$. When a four-term fit of the spectra is forced to include V_{Ti}'''' or V_{Sr}'' (see supplementary material Table I), a free term is still found between 198 and 266 ps, intermediate between the V_{Ti}'''' and V_{Sr}'' values, indicating that the dominant lifetime component is not solely a convolution of titanium and strontium vacancies as found in our previous measurements on PLD $SrTiO_3$ films.[9,10]

The titanium-oxygen vacancy complexes, TiO_x, identified by our PALS results, are likely charge neutral and explain the low loss properties of these tunable dielectric materials at high frequencies of applied electromagnetic fields.[31,32] Positrons trap both neutral or negative defects. In contrast, the trapping rate to positively charged open-

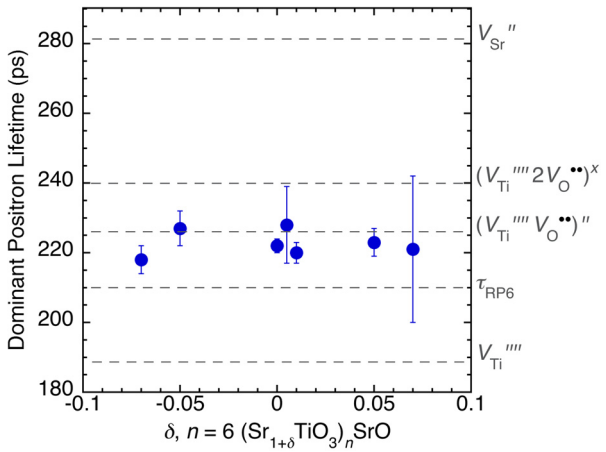

FIG. 2. The dominant positron lifetime from a free fit of the PALS spectra of the $n = 6$ $(Sr_{1+\delta}TiO_3)_nSrO$ thin-film stoichiometry series. Dashed lines show the characteristic lifetimes associated with possible defects in $SrTiO_3$ written using Kröger–Vink notation and τ_{RP6}, the bulk lifetime for $n = 6$ $(SrTiO_3)_nSrO$.

volume defects is negligible. Any vacancy defect is, in principle, a trap for positrons, but the Coulomb barrier presented by positively charged defects inhibits trapping.[45] In the case of TiO_2 ($x = 2$) vacancies, they are charge neutral and in essence regions of $(SrO)_2$ faults, seen as $SrTiO_3 + (V_{Ti}''''2V_O^{\bullet\bullet})^x = SrO$.[46] If they exist, vacancies of $(V_{Ti}''''V_O^{\bullet\bullet})''$, ($x = 1$), are also likely charge neutral with the addition of two electrons from nearby oxygen vacancies.[47,48] These results establish the ability of the $(SrTiO_3)_nSrO$ structure to mitigate defects and explain the exceptional performance of strained $(SrTiO_3)_nSrO$ films at gigahertz frequencies where loss has been identified to be due to charged point defects.[34–36]

The structural accommodations revealed by STEM-EELS support this interpretation of the PALS data. Dark boundaries between SrO planes in Figs. 1(c)–1(e) and 3 can easily be traced between regions of continuous perovskite, most notably as the boundaries between the $n = 6$ Ruddlesden–Popper layers. In general, atomic columns of strontium and titanium can be differentiated by their relative brightness, with heavy strontium atoms appearing brighter than comparatively lighter titanium sites. Areas where all atomic sites show similar contrast suggest projection through atomic columns containing both strontium and titanium, indicating regions that are crystallographically offset by $\frac{a}{2}[110]$ due to an $(SrO)_2$ Ruddlesden–Popper fault.

In the stoichiometric case, Figs. 1(d), 3(c), and 3(d), discrete $(SrO)_2$ layers are separated by clear gaps in the titanium elemental map where SrO planes form rock salt boundaries. The nominally stoichiometric film displays general adherence to the $n = 6$ Ruddlesden–Popper structure although some disruptions are observed as inclusions of vertical SrO planes and subtle crystalline defects like the step edge shown here.

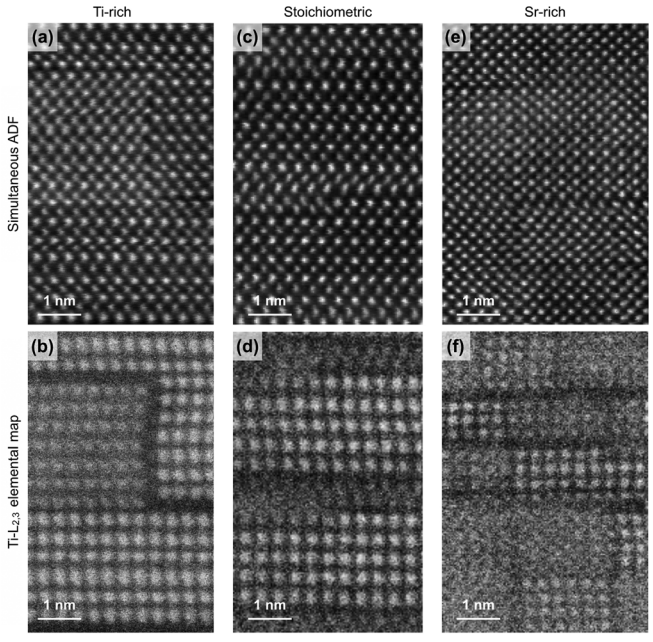

FIG. 3. Atomic-resolution EELS mapping of the Ti-$L_{2,3}$ edge highlights how the stoichiometric (c) and (d) Ruddlesden–Popper structure adapts to accommodate off-stoichiometry by forming (a) and (b) larger (titanium-rich with $\delta \sim -0.05$) or (e) and (f) smaller (strontium-rich with $\delta \sim +0.05$) blocks of continuous $SrTiO_3$ between SrO plane boundaries.

The titanium-rich (strontium-poor) film in Figs. 1(c), 3(a), and 3(b) shows how the Ruddlesden–Popper phase has adjusted to accommodate its off-stoichiometry: larger regions of continuous $SrTiO_3$ have formed as excess titanium fills in-between neighboring SrO rock salt layers (or, equivalently, as SrO rock salt boundaries are removed). The elemental map in Fig. 3(b) clearly shows regions of both higher n (upper right corner) and projection through an $(SrO)_2$ Ruddlesden–Popper fault along the growth direction (central region). The regions where the titanium atomic columns are clearly resolved (for example, at the upper right corner and lower half of the image) correspond to a coherent $SrTiO_3$-type structure where the TiO_2 planes are continuous in the electron projection direction (i.e., in and out of the page). The regions where titanium atomic contrast is less clear (as is the case for the central part of the image) indicate projection through two or more local $SrTiO_3$ structures offset relative to each other in the plane of the page by a half unit cell, as would form at a Ruddlesden–Popper boundary or the SrO rock salt planes between layers.

In contrast to the titanium-rich film, the strontium-rich film in Figs. 1(e), 3(e), and 3(f) forms extra SrO planes beyond the normal Ruddlesden–Popper phase, breaking up the $n = 6$ layers both horizontally and vertically into regions of locally smaller effective n, similar to effects observed in other strontium-rich $SrTiO_3$ films.[18] The titanium map of the strontium-rich film, Fig. 3(f), provides a clear view of extra SrO planes forming both vertically and horizontally, dividing Ruddlesden–Popper layers into "bricks" of much smaller effective n. The extra SrO planes, which are directly visible in the elemental map, form normal to the plane of the page. The regions of reduced titanium atomic contrast also indicate the formation of extra SrO planes parallel to the plane of the page, resulting in mixed projection through offset $SrTiO_3$ blocks as shown in Fig. 3(b).

The defect mitigating nature of $(SrTiO_3)_nSrO$ Ruddlesden–Popper phases was probed using PALS by introducing off-stoichiometric $Sr_{1+\delta}TiO_3$ into the Ruddlesden–Popper superlattice to form a series of 300 nm thick $n = 6$ $(Sr_{1+\delta}TiO_3)_nSrO$ thin films grown by MBE on (001) $SrTiO_3$. Atomic-resolution STEM and EELS show how off-stoichiometric films adjust structurally to accommodate either excess titanium (fewer SrO rock salt boundaries) or excess strontium (additional SrO rock salt boundaries). The lack of variance with off-stoichiometry seen in corresponding PALS spectra and the absence of trapping to strontium vacancies in titanium-rich films further support this conclusion that $(SrO)_2$ faults are indeed accommodating non-stoichiometry without dominant introduction of cation monovacancies as observed in PLD $Sr_{1+\delta}TiO_3$ thin films.[9,10] The observed TiO_x vacancies are likely charge neutral nano-regions of SrO faults, $SrTiO_3 + (V_{Ti}''''2V_O^{\bullet\bullet})^x = SrO$. Further studies on the contribution of oxygen vacancies and antisite defects, which cannot be fully studied using PALS, are needed to provide full understanding of the defect mechanisms in $(SrTiO_3)_nSrO$.

See the supplementary material for additional details on the PALS experimental setup, the mean positron lifetime plotted for the $n = 6$ $(Sr_{1+\delta}TiO_3)_nSrO$ thin film series, a table of positron lifetimes fitted from the PALS spectra for all samples, and further details of the DFT calculations of the positron characteristic lifetimes.

The synthesis science work at Cornell was supported by the U.S. Department of Energy, Office of Basic Sciences, Division of Materials Sciences and Engineering, under Award No. DE-SC0002334. Sample preparation was in part facilitated by the Cornell NanoScale Facility, a member of the National Nanotechnology Coordinated Infrastructure (NNCI), which was supported by the National Science Foundation (Grant No. NNCI-1542081). This work made use of the Cornell Center for Materials Research Shared Facilities, which are supported through the NSF MRSEC program (No. DMR-1719875). B.H.G. and L.F.K. acknowledge support from the Department of Defense Air Force Office of Scientific Research (No. FA 9550-16-1-0305). The FEI Titan Themis 300 was acquired through No. NSF-MRI-1429155, with additional support from Cornell University, the Weill Institute, and the Kavli Institute at Cornell. The Thermo Fisher Helios G4 X FIB was acquired with support by NSF No. DMR-1539918. D.J.K. gratefully acknowledges the financial support provided by FRM-II to perform the high-intensity positron beam measurements at Heinz Maier-Leibnitz Zentrum (MLZ), Garching, Germany.

DATA AVAILABILITY

The data that support the findings of this study are available in the supplementary material and from the corresponding author upon reasonable request.

REFERENCES

[1]H. Yamada and G. R. Miller, J. Solid State Chem. **6**, 169 (1973).
[2]S. Wiedigen, T. Kramer, M. Feuchter, I. Knorr, N. Nee, J. Hoffmann, M. Kamlah, C. A. Volkert, and C. Jooss, Appl. Phys. Lett. **100**, 061904 (2012).
[3]C. M. Brooks, R. B. Wilson, A. Schäfer, J. A. Mundy, M. E. Holtz, D. A. Muller, J. Schubert, D. G. Cahill, and D. G. Schlom, Appl. Phys. Lett. **107**, 051902 (2015).
[4]D.-W. Oh, J. Ravichandran, C.-W. Liang, W. Siemons, B. Jalan, C. M. Brooks, M. Huijben, D. G. Schlom, S. Stemmer, L. W. Martin, A. Majumdar, R. Ramesh, and D. G. Cahill, Appl. Phys. Lett. **98**, 221904 (2011).
[5]D. Lee, H. Lu, Y. Gu, S.-Y. Choi, S.-D. Li, S. Ryu, T. R. Paudel, K. Song, E. Mikheev, S. Lee, S. Stemmer, D. A. Tenne, S. H. Oh, E. Y. Tsymbal, X. Wu, L.-Q. Chen, A. Gruverman, and C. B. Eom, Science **349**, 1314 (2015).
[6]T. Tanaka, K. Matsunaga, Y. Ikuhara, and T. Yamamoto, Phys. Rev. B **68**, 205213 (2003).
[7]D. Freedman, D. Roundy, and T. Arias, Phys. Rev. B **80**, 064108 (2009).
[8]T. Suzuki, Y. Nishi, and M. Fujimoto, Philos. Mag. A **80**, 621 (2000).
[9]D. J. Keeble, S. Wicklein, R. Dittmann, L. Ravelli, R. A. Mackie, and W. Egger, Phys. Rev. Lett. **105**, 226102 (2010).
[10]D. J. Keeble, S. Wicklein, L. Jin, C. L. Jia, W. Egger, and R. Dittmann, Phys. Rev. B **87**, 195409 (2013).
[11]D. Lee, H. Wang, B. A. Noesges, T. J. Asel, J. Pan, J.-W. Lee, Q. Yan, L. J. Brillson, X. Wu, and C.-B. Eom, Phys. Rev. Mater. **2**, 060403 (2018).
[12]D. Balz and K. Plieth, Z. Electrochem. **59**, 545 (1955).
[13]S. N. Ruddlesden and P. Popper, Acta Crystallogr. **10**, 538 (1957).
[14]S. N. Ruddlesden and P. Popper, Acta Crystallogr. **11**, 54 (1958).
[15]T. Ohnishi and M. Lippmaa, Appl. Phys. Lett. **87**, 241919 (2005).
[16]T. Ohnishi, K. Shibuya, T. Yamamoto, and M. Lippmaa, J. Appl. Phys. **103**, 103703 (2008).
[17]C. Xu, H. Du, A. J. H. van der Torren, J. Aarts, C.-L. Jia, and R. Dittmann, Sci. Rep. **6**, 38296 (2016).
[18]C. M. Brooks, L. Fitting Kourkoutis, T. Heeg, J. Schubert, D. A. Muller, and D. G. Schlom, Appl. Phys. Lett. **94**, 162905 (2009).
[19]S. Witek, D. M. Smyth, and H. Pickup, J. Am. Ceram. Soc. **67**, 372 (1984).
[20]L. J. Knott, N. J. Cockroft, and J. C. Wright, Phys. Rev. B **51**, 5649 (1995).
[21]J. G. Bednorz and K. A. Müller, Z. Phys. B **64**, 189 (1986).
[22]H. M. Buschbaum, Angew. Chem., Int. Ed. **28**, 1472 (1989).
[23]Y. Maeno, H. Hashimoto, K. Yoshida, S. Nishizaki, T. Fujita, J. G. Bednorz, and F. Lichtenberg, Nature **372**, 532 (1994).
[24]T. L. Meyer, R. Jacobs, D. Lee, L. Jiang, J. W. Freeland, C. Sohn, T. Egami, D. Morgan, and H. N. Lee, Nat. Commun. **9**, 92 (2018).
[25]Y. Moritomo, A. Asamitsu, H. Kuwahara, and Y. Tokura, Nature **380**, 141 (1996).
[26]T. Birol, N. A. Benedek, and C. J. Fennie, Phys. Rev. Lett. **107**, 257602 (2011).
[27]M. J. Pitcher, P. Mandal, M. S. Dyer, J. Alaria, P. Borisov, H. Niu, J. B. Claridge, and M. J. Rosseinsky, Science **347**, 420 (2015).
[28]Y. S. Oh, X. Luo, F.-T. Huang, Y. Wang, and S.-W. Cheong, Nat. Mater. **14**, 407 (2015).
[29]N. A. Benedek, J. M. Rondinelli, H. Djani, P. Ghosez, and P. Lightfoot, Dalton Trans. **44**, 10543 (2015).
[30]P. V. Balachandran, J. Young, T. Lookman, and J. M. Rondinelli, Nat. Commun. **8**, 14282 (2017).
[31]C.-H. Lee, N. D. Orloff, T. Birol, Y. Zhu, V. Goian, E. Rocas, R. Haislmaier, E. Vlahos, J. A. Mundy, L. F. Kourkoutis, Y. Nie, M. D. Biegalski, J. Zhang, M. Bernhagen, N. A. Benedek, Y. Kim, J. D. Brock, R. Uecker, X. X. Xi, V. Gopalan, D. Nuzhnyy, S. Kamba, D. A. Muller, I. Takeuchi, J. C. Booth, C. J. Fennie, and D. G. Schlom, Nature **502**, 532 (2013).
[32]N. M. Dawley, E. J. Marksz, A. M. Hagerstrom, G. H. Olsen, M. E. Holtz, V. Goian, C. Kadlecch, J. Zhang, X. Lu, J. A. Drisko, R. Uecker, S. Ganschow, C. J. Long, J. C. Booth, S. Kamba, C. J. Fennie, D. A. Muller, N. D. Orloff, and D. G. Schlom, Nat. Mater. **19**, 176 (2020).
[33]G. Amow, I. J. Davidson, and S. J. Skinner, Solid State Ionics **177**, 1205 (2006).
[34]C. Elissalde and J. Ravez, J. Mater. Chem. **11**, 1957 (2001).
[35]A. K. Tagantsev, V. O. Sherman, K. F. Astafiev, J. Venkatesh, and N. Setter, J. Electroceram. **11**, 5 (2003).
[36]A. Vorobiev, P. Rundqvist, K. Khamchane, and S. Gevorgian, J. Appl. Phys. **96**, 4642 (2004).
[37]M. A. Mccoy, R. W. Grimes, and W. E. Lee, Philos. Mag. A **75**, 833 (1997).
[38]J. H. Haeni, C. D. Theis, and D. G. Schlom, J. Electroceram. **4**, 385 (2000).
[39]R. C. Haislmaier, G. Stone, N. Alem, and R. Engel-Herbert, Appl. Phys. Lett. **109**, 043102 (2016).
[40]M. Barone, N. M. Dawley, H. Nair, M. Holtz, A. Soukiassian, K. Lee, Y. Jia, T. Heeg, R. Gatt, Y. Nie, and D. G. Schlom, "A superlattice approach to analyze the x-ray diffraction of Ruddlesden-Popper films" (unpublished).
[41]P. Sperr, W. Egger, G. Kogel, G. Dollinger, C. Hugenschmidt, R. Repper, and C. Piochacz, Appl. Surf. Sci. **255**, 35 (2008).
[42]C. Hugenschmidt, B. Lowe, J. Mayer, C. Piochacz, P. Pikart, R. Repper, M. Stadlbauer, and K. Schreckenbach, Nucl. Instrum. Methods Phys. Res., Sect. A **593**, 616 (2008).
[43]D. J. Keeble, R. A. Mackie, W. Egger, B. Löwe, P. Pikart, C. Hugenschmidt, and T. J. Jackson, Phys. Rev. B **81**, 064102 (2010).
[44]T. Torsti, T. Eirola, J. Enkovaara, T. Hakala, P. Havu, V. Havu, T. Hoynalanmaa, J. Ignatius, M. Lyly, I. Makkonen, T. T. Rantala, J. Ruokolainen, K. Ruotsalainen, E. Rasanen, H. Saarikoski, and M. J. Puska, Phys. Status Solidi B **243**, 1016 (2006).
[45]M. J. Puska, C. Corbel, and R. M. Nieminen, Phys. Rev. B **41**, 9980 (1990).
[46]U. Balachandran and N. G. Eror, J. Mater. Sci. **17**, 2133 (1982).
[47]A. Janotti, J. B. Varley, M. Choi, and C. G. Van de Walle, Phys. Rev. B **90**, 085202 (2014).
[48]M. E. Zvanut, S. Jeddy, E. Towett, G. M. Janowski, C. Brooks, and D. G. Schlom, J. Appl. Phys. **104**, 064122 (2008).

Supplementary Information

Defect accommodation in off-stoichiometric $(SrTiO_3)_nSrO$ Ruddlesden-Popper superlattices studied with positron annihilation spectroscopy

Positron annihilation lifetime spectroscopy experiments

Experimental variable energy positron annihilation lifetime spectroscopy (VE-PALS) measurements were performed on seven $n = 6$ $(Sr_{1+\delta}TiO_3)_nSrO$ films with δ varying from –0.07 to +0.07 using the PLEPS instrument on the neutron induced positron beamline (NEPOMUC) operated by FRM II at the Heinz Maier-Leibnitz Zentrum (MLZ), Garching. Measurements were performed for positron implantation energies of 4, 5, and 6 keV. Each spectrum contained 4×10^6 counts and the instrument resolution function was described by the sum of three Gaussians and had a shape parameter full-width-half-maximum varying from 203 to 276 ps over the period of the measurements. The spectra were fitting using the package PALSfit v3.195 from the Technical University of Denmark.[1] The detailed fits obtained for the seven 5 kV spectra are given in Table I. The mean positron lifetimes, obtained from the four lifetime free fits, are shown in FIG. S1. The mean positron lifetime is the sum of all of the lifetime components obtained, each weighted by the intensity of that component. The mean positron lifetime is in principle independent of the number of lifetime components used in the deconvolution. The dominant lifetime component shown in FIG. 2 is more characteristic of the dominant open-volume defect population contributing to the positron annihilation lifetime spectrum.

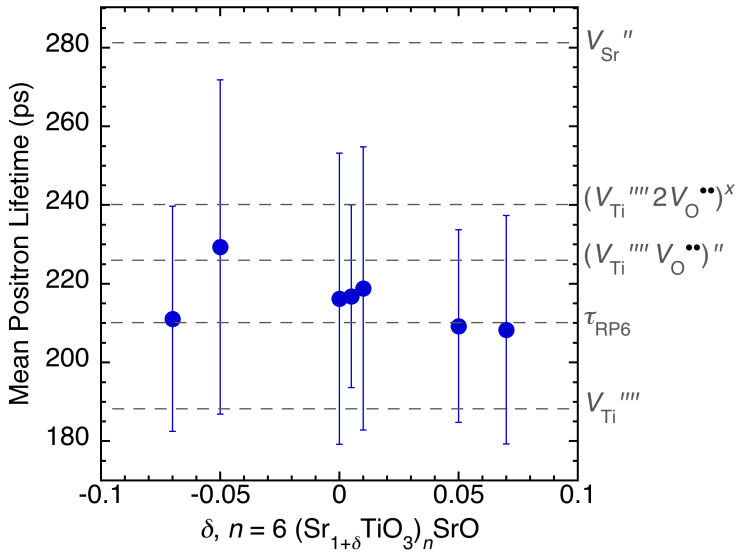

FIG S1. Mean positron lifetime values obtained for 5 keV spectra from near-stoichiometric n = 6 $(Sr_{1+\delta}TiO_3)_nSrO$ Ruddlesden-Popper films assuming four components using PALSfit.

Table S1 Positron lifetime component values obtained for 5 keV spectra from near-stoichiometric n = 6 $(Sr_{1+\delta}TiO_3)_nSrO$ Ruddlesden-Popper films using PALSfit. If a fit component value is fixed this is denoted by F. Fits were performed assuming four lifetime components, but three lifetime (3L) free fits are also included for comparison.

Sample	**Fit**	τ_1 **(ps)**	I_1 **(%)**	τ_2 **(ps)**	I_2 **(%)**	τ_3 **(ps)**	I_3 **(%)**	χ^2
Titanium rich / strontium poor, n = 6 $(Sr_{1+\delta}TiO_3)_nSrO$								
δ = -0.07	Free fit	107(11)	11(3)	218(4)	88(2)	469(70)	1.5(8)	0.965
NMD361	Free fit (3L)	156(5)	36(4)	239(3)	64(4)	1306(97)	0.15(2)	0.995
	V_{Sr}'' fixed	33(18)	4(1)	194(2)	75(1)	281F	21(1)	1.050
	V_{Ti}'''' fixed	183F	63(2)	257(5)	37(2)	747(366)	0.2(2)	1.058
	V_{Ti}'''' & V_{Sr}'' fixed	183F	63(6)	236(36)	20(3)	281F	18(9)	1.064
δ = -0.05	Free fit	80(16)	6(2)	227(5)	87(3)	358(36)	7(4)	1.120
NMD397	Free fit (3L)	157(6)	27(3)	254(3)	73(3)	1036(104)	0.15(4)	1.147
	V_{Sr}'' fixed	22(39)	5(6)	202(2)	58(4)	281F	35(1)	1.132
	V_{Ti}'''' fixed	183F	44(1)	266(2)	56(1)	789(249)	0.2(1)	1.158
	V_{Ti}'''' & V_{Sr}'' fixed	183F	40(7)	237(29)	27(4)	281F	33(10)	1.144

Stoichiometric, n = 6 ($Sr_{1+\delta}TiO_3)_nSrO$								
δ = 0	Free fit	102(11)	7(2)	222(2)	92(1)	571(66)	0.9(3)	1.054
NMD330	Free fit (3L)	133(8)	14(2)	229(2)	85(2)	913(47)	0.32(4)	1.081
	V_{Sr}'' fixed	117(65)	5(8)	206(9)	75(5)	281F	20(3)	0.914
	V_{Ti}'''' fixed	183F	50(3)	249(5)	50(3)	688(436)	0.2(3)	0.913
	V_{Ti}'''' & V_{Sr}'' fixed	183F	48(7)	235(21)	37(3)	281F	15(9)	0.916
δ = 0	Free fit	161(27)	22(19)	228(11)	77(19)	494(80)	1.0(8)	0.991
NMD399	Free fit (3L)	204(2)	89(3)	315(13)	11(3)	2014(486)	0.03(1)	1.023
	V_{Sr}'' fixed	91(77)	2(3)	201(5)	78(1)	281F	20(2)	0.987
	V_{Ti}'''' fixed	183F	50(3)	245(5)	50(3)	574(136)	0.5(4)	0.979
	V_{Ti}'''' & V_{Sr}'' fixed	183F	44(12)	222(20)	39(7)	281F	17(6)	0.988
Strontium rich / titanium poor, n = 6 ($Sr_{1+\delta}TiO_3)_nSrO$								
δ = 0.01	Free fit	98(14)	8(2)	220(3)	90(2)	524(54)	1.7(5)	1.065
NMD355	Free fit (3L)	184(4)	63(5)	269(6)	37(5)	1597(86)	0.21(2)	1.120
	V_{Sr}'' fixed	193(2)	74(1)	281F	25(2)	905(323)	0.3(1)	1.113
	V_{Ti}'''' fixed	183F	54(3)	252(5)	46(2)	677(155)	642(298)	1.093
	V_{Ti}'''' & V_{Sr}'' fixed	183F	56(9)	228(38)	20(3)	281F	24(7)	1.120
δ = 0.05	Free fit	141(12)	21(6)	223(4)	79(6)	630(81)	0.5(2)	1.000
NMD394	Free fit (3L)	170(5)	49(6)	244(5)	51(6)	1637(149)	0.09(1)	1.026
	V_{Sr}'' fixed	54(20)	5(1)	197(20)	79(1)	281F	17(1)	0.970
	V_{Ti}'''' fixed	89(49)	2(2)	183F	59(6)	252(5)	38(4)	0.993
	V_{Ti}'''' & V_{Sr}'' fixed	183F	65(4)	254(32)	30(22)	281F	4(26)	0.982
δ = 0.07	Free fit	161(32)	28(19)	221(21)	71(34)	457(199)	1(2)	1.001
NMD392	Free fit (3L)	188(3)	77(6)	267(9)	23(6)	2117(178)	0.10(1)	1.004
	V_{Sr}'' fixed	53(47)	2(1)	194(17)	83(1)	281F	15(1)	1.022
	V_{Ti}'''' fixed	183F	65(3)	249(7)	34(2)	610(471)	0.2(4)	1.022
	V_{Ti}'''' & V_{Sr}'' fixed	183F	64(7)	231(25)	25(2)	281F	11(6)	1.024

Positron lifetime calculations

The calculations were performed with the MIKA/Doppler package, where the electron density of the solid is approximated by the non-self-consistent superposition of free atom electron densities in the absence of the positron (the so-called 'conventional scheme'). This approximation to the complete two-component density functional theory (TCDFT) has been found to give positron lifetimes close to TCDFT as well as experimental values. The electron-positron enhancement factor obtained from the data of Arponen and Pajanne,[2] parameterization by Boronski and Nieminen (BN),[3] described within the local density approximation (LDA), and with an expression obtained by Barbiellini and co-workers,[4,5] (referred to as AP) described within the generalized gradient approximation (GGA) were used. Calculations were performed using a 512 atom supercell of $n = 6$ $(Sr_1TiO_3)_nSrO$ Ruddlesden-Popper phase structure, the resulting bulk positron lifetime value was 208 ps. A similar calculation for a 1080 atom supercell of $SrTiO_3$ gave a value of 151 ps, in agreement with previous work.[6] Calculations were also performed using a similar super cell size for the $(V_{Ti}''''V_O^{\bullet\bullet})''$ divacancy defect, and for a linear $(V_O^{\bullet\bullet}V_{Ti}''''V_O^{\bullet\bullet})^x$ trivacancy complexes in $SrTiO_3$, these yielded values of 226 ps and 240 ps, respectively. The latter value is slightly smaller than the previously reported value of 247 ps.[7] In these calculations involving titanium vacancy related defects, the geometry of the defects were not relaxed.

References

1. J. V. Olsen, P. Kirkegaard, N. J. Pedersen, and M. Eldrup, Phys. Status Solidi C **4**, 4004 (2007).

2. J. Arponen and E. Pajanne, Annals of Physics **121**, 343 (1979).

3. E. Boronski and R. M. Nieminen, Phys. Rev. B **34**, 3820 (1986).

4. B. Barbiellini, M. J. Puska, T. Korhonen, A. Harju, T. Torsti, and R. M. Nieminen, Phys. Rev. B **53**, 16201 (1996).

5. B. Barbiellini, M. J. Puska, T. Torsti, and R. M. Nieminen, Phys. Rev. B **51**, 7341 (1995).

6. D. J. Keeble, S. Wicklein, R. Dittmann, L. Ravelli, R. A. Mackie, and W. Egger, Phys. Rev. Lett. **105**, 226102 (2010).

7. D. J. Keeble, R. A. Mackie, W. Egger, B. Löwe, P. Pikart, C. Hugenschmidt, and T. J. Jackson, Phys. Rev. B **81**, 064102 (2010).